Electrochimica Acta 467 (2023) 143058

Contents lists available at ScienceDirect

Electrochimica Acta

journal homepage: www.journals.elsevier.com/electrochimica-acta

Nanostructured Ir-based electrocatalysts for oxygen evolution prepared by galvanic displacement of Co and Ni

Freja Bech Holde [a], Paula Sebastián-Pascual [a,*], Kim Nicole Dalby [b], Elvira Gómez [c], María Escudero-Escribano [a,d,e,*]

[a] Department of Chemistry, University of Copenhagen, Universitetsparken 5, 2100 Copenhagen, Denmark
[b] Topsoe A/S, Haldor Topsøes Allé 1, DK-2800 Kgs. Lyngby, Denmark
[c] Departament de Ciència de Materials i Química Física, Universitat de Barcelona, Martí i Franquès, 1, Barcelona 08028, Spain
[d] Catalan Institute of Nanoscience and Nanotechnology (ICN2), CSIC, Barcelona Institute of Science and Technology, UAB Campus, 08193 Bellaterra, Barcelona, Spain
[e] ICREA, Pg. Lluís Companys 23, 08010 Barcelona, Spain

ARTICLE INFO

Keywords:
Electrodeposition
Deep eutectic solvent
Galvanic displacement reaction
Iridium oxide
Oxygen evolution reaction

ABSTRACT

Proton exchange membrane (PEM) electrolysers are promising devices to produce hydrogen as a green fuel. Currently, this technology is limited by the sluggish kinetics of the oxygen evolution reaction (OER). In this work, we describe an environmentally safe method for the preparation of Ir oxide thin films (IrO_2) for OER. Electrodeposition of Co and Ni was performed in the non-toxic choline chloride:urea deep eutectic solvent (ChCl:urea DES), followed by galvanic displacement reaction (GDR) of Co and Ni by Ir(IV). We evaluated how the GDR conditions, such as the metal replaced (Co or Ni), time and temperature affect both the activity and stability of the deposited IrO_2 films on gold substrates. We observed that GDR of Ni at 90 °C induces morphological changes on the IrO_2 nanostructures which resulted in higher activity and stability towards OER. We highlight that not only reducing mass loadings of Ir but also tuning the surface morphology and structure controlling the synthesis preparation, as well as investigating the role of the substrate, are key to design more active and stable OER electrocatalysts.

1. Introduction

The scarcity and decline of fossil fuels make the transition towards a zero-carbon emission economy more urgent [1–3]. The so-called hydrogen economy, which uses hydrogen as an energy carrier, is a potential and green solution to replace fossil fuels, where water is the only by-product formed when hydrogen and oxygen are consumed in fuel cells [4–6].

In proton exchange membrane water electrolysers (PEMWEs), operating under acidic conditions, the production of hydrogen is fast in relation to alkaline exchange membrane electrolysers [7,8]. However, the technology needs to overcome other challenges to become economically competitive in the long term. One of the main bottlenecks of PEM water electrolysers lies in the slow kinetics of the reaction at the anode, i.e., the oxygen evolution reaction (OER), as it requires high applied energy input to achieve high current densities [6,9–11]. As a result, high amounts of oxides based on scarce iridium are required at the PEM electrolyser anode. While Ir oxide electrocatalysts are reasonably active and stable, Ru oxides are rather unstable under reaction conditions, as they dissolve rapidly under reduction conditions in acidic solution [12,13]. Finding new synthesis procedures that minimize the environmental and energetic costs is important for achieving a transition to a sustainable economy [1].

Different methods have been reported to prepare Ir and Ir oxide nanocatalysts with variable size and morphology, aiming to maximize the area and minimize metal loadings for more active and stable OER electrocatalysis [14–19]. Colloidal synthesis of Ir nanoparticles (NPs) allows for the preparation of NPs of small size down to 3 nm, although generally via using surfactant agents to avoid particle agglomeration [20,21]. The use of surfactant agents means they need to be removed as they block the active sites. Some agents are harmful to the environment, and, in addition, the removal steps of most surfactants are time and energy consuming [20–22]. We recently showed the preparation of self-supported Ir porous networks by alternating the deposition of Ir and Co by physical vapour deposition (PVP), followed by acidic leaching of the Co [23]. The obtained three-dimensional Ir networks showed high

* Corresponding authors.
E-mail addresses: paula.pascual@chem.ku.dk (P. Sebastián-Pascual), maria.escudero@icn2.cat, maria.escudero@chem.ku.dk (M. Escudero-Escribano).

https://doi.org/10.1016/j.electacta.2023.143058
Received 12 March 2023; Received in revised form 11 August 2023; Accepted 19 August 2023
Available online 20 August 2023

mass activities of ca. 2000 Ag^{-1} at 1.55 V vs RHE due to enhancement of the electroactive surface area of the Ir porous layer. Electrochemical methods combining Ir with less noble metals, such as Co or Ni, for the preparation of new Ir catalyst structures, have previously been explored as well. Alia *et al.* developed a simple methodology for the preparation of Ir nanowires via galvanic displacement reaction (GDR) of Co or Ni nanowires by Ir(IV) ions [24]. Metallic Co or Ni nanowires were replaced by Ir(IV), forming metallic Ir nanowires with one of the highest reported both mass activities (8000 Ag^{-1} at 1.55 V vs RHE) in the literature, and enhanced stability after leaching of the Co and Ni. Galvanic displacement reactions of Co and Ni by Ir(IV) occur spontaneously, i.e., without applying any voltage input, because the standard redox potential of Ir ($E^0_{Ir/Ir4+}$=0.86 V vs RHE) overcomes the standard redox potential of either Co or Ni ($E^\circ_{Co/Co2+}$= −0.280 V vs RHE and $E^0_{Ni/Ni2+}$= −0.257 V vs RHE) [24–26].

In this work, we introduce a feasible methodology to prepare Ir nanostructured thin films via galvanic displacement of electrodeposited Co and Ni in a choline chloride deep eutectic solvent (DES). DESs are classified as green solvents due to their high biocompatibility and biodegradability, easy synthesis, low cost, and high availability of raw materials, and have been widely used in the field of metal electrodeposition [27–32]. Electrodeposition is a versatile technique that allows the deposition of films by simply modulating the applied potential conditions, and is advantageous to modify substrates with variable shape or geometry if they are conductive [33]. The electroplating technique has been widely used in the coating industry [34,35], and has been employed for direct modification of several types of surface electrodes, even gas diffusion electrodes (GDE) or membrane assembly electrodes (MEA) for PEM using pulse electrodeposition [36,37]. We used gold substrates that we coated with Co or Ni via electrodeposition in a choline chloride urea DES. Then, we deposited Ir nanostructures via galvanic displacement reaction of Co and Ni by immersing the coated substrates in an $IrCl_4$ solution. We used gold beads and gold planar sheets (*Si/Ti/Au* sheets) to evaluate substrates of different shapes with IrO_2 thin films. We have assessed how the GDR conditions, such as temperature, time and loadings of deposited Co and Ni, affected the growth of the IrO_2 films, and their OER activity and stability. In the discussion, we elaborate on the potential uses and challenges regarding our catalysts as well as discuss their application in relation to other types of OER anodes.

2. Experimental

2.1. Preparation of Co and Ni deposits in DES

Metallic Co and Ni surfaces were prepared by electrodeposition technique in a DES solution, following previously reported protocols [30,31]. The DES solution was prepared by mixing choline chloride (ChCl, Across Organics, 99%) and urea (Sigma-Aldrich, 99%) in a 1:2 molar ratio at 40 °C under constant stirring. Both $CoCl_2$ and $NiCl_2$ salts were purchased from Alfa Aesar (Cobalt(II)chloride, 99% purity and Nickel(II) chloride, 99% purity). The 0.1 M $CoCl_2$ + DES or 0.1 M $NiCl_2$ + DES bath solutions for metal electrodeposition were prepared by drying the salts and dissolving them in DES under stirring conditions at 70 °C in dry glassware. The bath solutions were bubbled with Ar gas for 3 h before experiments, to remove excess water and prevent further moistening. We performed the Co and Ni electrodeposition at 70 °C in a small volume thermostatic cell with three electrodes, which contained 1–2 mL of bath solution. The metal electrodeposition was carried out at 70 °C to accelerate the rate deposition without solvent Co—reduction [30–32]. Circulated charges of −10 mC, −15 mC and −25 mC were obtained during deposition. We used the circulated charges during the chronoamperometric electrodeposition to estimate the loadings of Co and Ni (μg cm^{-2}) in the nanostructures. A gold wire was used as the counter electrode and a silver wire as a quasi-reference electrode. The gold beads and the gold and silver wires were pre-treated by flame annealing and cooled down in air. The polycrystalline gold beads were prepared following the Clavilier's method [38], where a gold wire was slowly melted until a bead shape appeared and then cooled down.

2.2. Preparation of IrO_2 nanostructured films

Ir—Co and Ir—Ni catalysts on polycrystalline gold beads were prepared via galvanic displacement reaction (GDR) of deposited Co or Ni by Ir(IV) ions. For the GDR, the Co- or Ni-deposited polycrystalline gold beads were immersed in solutions of $IrCl_4$ salt (Iridium(IV) chloride, Alfa Aesar, 99%) immediately after metal electrodeposition. For the Co replacement, the Ir(IV) solution had a concentration of 2–4 mM and was kept at room temperature (RT). The time of immersion differed from 6 to 12 min depending on the circulated charge of deposited Co. For the Ni replacement, the Ir(IV) solution had a concentration between 4 and 8 mM $IrCl_4$ and was heated to 90 °C during the galvanic displacement reaction to accelerate the reaction kinetics. The time of immersion was also increased to 30–60 min. In all cases, the GDR time was selected to ensure that Co and Ni replacement by Ir(IV) was close to 100%. After GDR, the Ir—Co—Au and Ir—Ni-Au electrodes were then treated in a 1:1 solution of nitric acid (VWR, 68%) to remove or leach the traces of Co and Ni [23,24]. To calculate the nominal loading of IrO_2, we used the Faraday law [39] to relate the total amount of moles of Ir replacing the moles of deposited Co and Ni, with the circulated charge during the deposition of Co and Ni, accepting that in the selected electrodeposition conditions the deposition efficiency is close to 100%. The equation $m_{Ir} = Q_{Co/Ni} * M_{Ir}/znF$ was used to estimate the nominal loading of Ir. Q represents the circulated charge of Co and Ni, z is the number of transferred electrons in the reduction of the ionic metals M^{z+} (2 electrons are transferred in the reduction of Co(II) and of Ni(II) during the electrodeposition), n is the number of moles involved in the galvanic displacement (2 mol of Co or Ni is replaced by 1 mole of Ir) and, F is the Faraday constant (F = 96,500 C/mol e^-). Considering the GDR of Co and Ni by Ir:

$$2Co + Ir^{4+} \rightarrow 2Co^{2+} + Ir$$

$$2Ni + Ir^{4+} \rightarrow 2Ni^{2+} + Ir$$

If all the Co and Ni is replaced, we estimated an Ir loading of 12.4 μg for a circulated charge of −25 mC, 7.5 μg Ir for a circulated charge of −15 mC and 5.0 μg for a circulated charge of −10 mC. The actual loading of Ir and the efficiency of the GDR was then calculated by determining the real amount of Ir in the electrolyte by inductively coupled plasma mass spectrometry (ICP-MS). Samples of 1 mL were taken directly from the cell after electrochemical dissolution of the Ir film before ICP-MS measurements were done. The ICP-MS analysis was performed using the model Bruker Aurora Elite ICP-MS instrument.

2.3. Electrochemical measurements

Electrochemical characterization and conditioning of the Ir catalysts were performed in a standard three-electrode cell set-up containing 0.1 M $HClO_4$ (suprapure perchloric acid, Merck, 96%) electrolyte. A gold wire, previously flame-annealed, was used as counter electrode. As a reference electrode, we used a reversible hydrogen electrode (RHE) that we made by placing a Pt wire inside a glass tube with electrolyte saturated with H_2. The electrolyte was saturated with Ar before electrochemical measurements of the electrode commenced.

Before coating the gold bead surface with Ir, we carried out the base cyclic voltammetry of the bare gold bead in the 0.1 M $HClO_4$ electrolyte at 50 mV/s between 0 V and 1.7 V vs RHE. The surface area of the beads were then determined following the protocol as described by Trasatti et al [40] as described in the supplementary information, S.I, in Figure S1A.The gold bead surface areas were between 0.15–0.19 cm^2.

The electrochemically active surface area (ECSA) of the Ir catalysts was calculated by assessing the voltammetric hydrogen underpotential

deposition (HUPD) region recorded between 0.025 V and 0.5 V vs RHE at 50 mV/s in 0.1 M $HClO_4$ (Figure S1B). The determination of the areas (both geometric area (GA) and ECSA) is based on the work of Trasatti et al [40] and detailed by Lukaszewski et al [41] as well as based on the previous work by Arminio-Ravelo et al [20]. Details on the calculation for the ECSA can be found in the S.I. section S1B.

IrO_2 catalysts were then prepared by electrochemical conditioning consisting of continuous cycling at 500 mV/s in the potential range between 0.05 and 1.47 V vs RHE until a stable base cyclic voltammogram (CV) was achieved (Figure S1C). The extended double layer region of the IrO_2 catalysts was evaluated at 50 mV/s in the same potential range. We recorded cycles between 1.4 to 1.85 V to assess the OER activity. The potential of the anodic curves of the OER were IR_s—corrected *ex situ,* where I is the recorded current and R_s is the solution resistance. The solution resistance, R_s, was measured by means of impedance spectroscopy and ranged between 25 and 35 Ω. Chronoamperometric stability tests were done for 14 h at applied potentials of 1.6 V vs RHE for different Ir mass loadings. We saw no change in the chronoamperometric stability tests with or without constant Ar flow. Therefore, the electrolyte was only saturated with Ar before experiments were carried out. Chronopotentiometric tests were done by holding a constant current density of 11–14 mA/cm^2 until the potential reached that of gold OER activity (2.1 V vs RHE). All electrochemical experiments were performed using the Bio-Logic E-lab potentiostat and software.

2.4. Analysis of surface structure and morphology

Simultaneous field emission scanning electron microscopy (FE-SEM) and energy-dispersive x-ray spectroscopy (EDX) was performed to analyse the morphology and chemical composition of the samples. For this, the high-resolution Zeiss Gemini 500 FE-SEM at Topsoe A/S was used. Inlens and SE2 detectors were used at low voltages (2 keV) for high resolution imaging. A third detector, a Thermo Scientific UltraDry silicon drift detector, was used for collecting EDX data at higher voltages (15 keV) and the results were processed using Pathfinder Software.

3. Results

3.1. Preparation of the IrO_2 surfaces by galvanic displacement of Co or Ni

Fig. 1 illustrates the protocol employed to prepare the metallic Ir thin films via galvanic displacement reaction (GDR) of electrodeposited Co and Ni on gold bead substrates. The same preparation was used for the *Si/Ti/Au* substrates coated by Ir. The Ni(II) and Co(II) cations were reduced on the gold surface by applying a negative potential resulting in a thin, dark grey layer of Co or Ni, as seen in Fig. 1. We carried out both chronoamperometry (CA) and cyclic voltammetry to determine the potential range, which allows for controlled electrodeposition of metallic Co and Ni films at moderate rates and high efficiency. Details of the Co and Ni electrodeposition can be found in the S2 section (S.I.). Figures S2*a* and *b* show, respectively, the CVs before electrodeposition of the Co and Ni electrodeposition recorded at three different potential limits.

Figures S2*c* and S2*d* show the chronoamperometric profiles (*j-t* transients) during electrodeposition at different applied potentials between −0.6 V and −0.8 V vs Ag. For controlled growth of the metallic Ni and Co deposit on gold, and to ensure the formation of metallic Co and Ni deposits – critical for efficient GDR by Ir, we performed the Co and Ni electrodeposition at overpotentials near to −0.70 V vs Ag. At these applied potentials, the maximum current value is reached at around 90–120 s. We stopped applying potential when the preferred circulated charge was reached. A quasi-reference silver electrode was used for these measurements for ease in the heart-shaped cell design. The CV was always checked before performing the deposition with chronoamperomety. The rate of the deposition was kept similar for all measurements, meaning that the applied electrodepositon overpotential was the same. The Ag quasi reference electrode behaved stable during the measurements, and it should not influence the deposits.

After the preparation of the Co and Ni metallic films, we initiated the galvanic displacement reaction (GDR) of Co and Ni by Ir to prepare the metallic Ir deposit. We assessed how the loading of Co and Ni, time and heating conditions during the GDR influenced the formation of the IrO_2 thin film layer. We named the samples prepared from GDR of Co and Ni as Ir—Co and Ir—Ni, respectively. The Ir catalysts prepared from the galvanic displacement (GD) of Co films (Ir—Co) exhibited a red-golden colour, whereas the ones prepared from the Ni films (Ir—Ni) exhibited a dark grey colour as shown in Fig. 1.

After successful galvanic displacement of Co and Ni by Ir, we investigated the Ir deposits electrochemically. The left side panels in Fig. 2*a, b* and *c* compare the base cyclic voltammograms (CVs) in 0.1 M $HClO_4$ of metallic Ir—Co and Ir—Ni catalysts after leaching, prepared under different conditions, in the potential range between 0.0 V and 0.55 V vs RHE. The corresponding IrO_2, formed after continuous electrochemical cycling of the metallic Ir film in the potential range between 0.05 V and 1.47 V vs RHE, appear in the right-side panels of Fig. 2*a, b* and *c* (solid lines). Fig. 2*a* shows the CVs of Ir catalysts prepared with two different loadings of electrodeposited Co at −25 mC (dark blue line) and at −15 mC (light blue line). The metallic Ir CVs in the left panel

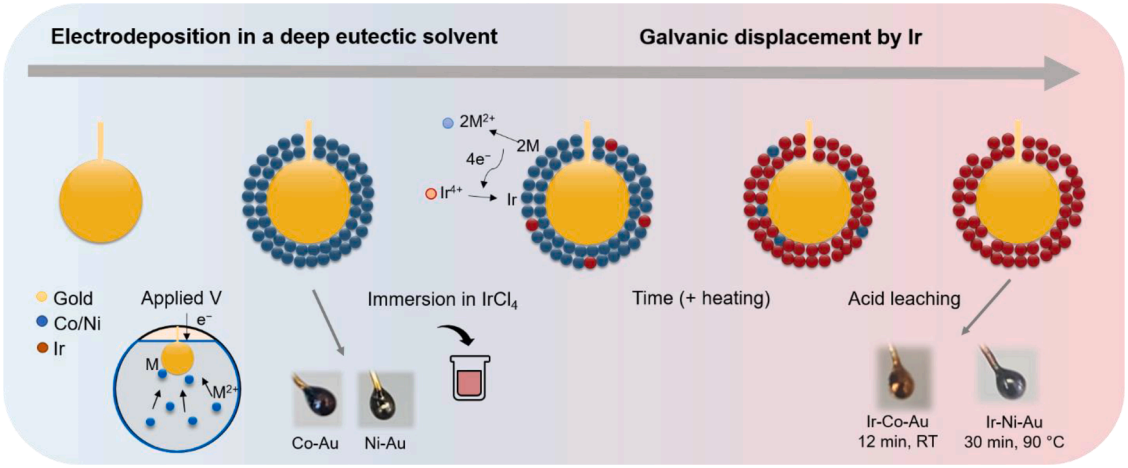

Fig. 1. Schematic of the experimental preparation of the Ir and Ir catalysts from the Co and Ni deposited surfaces. The Co—Au and Ni—Au beads were prepared by electrodeposition in a deep eutectic solvent. The beads were then immersed in $IrCl_4$ for galvanic displacement of Co and Ni by Ir and subsequently leached in nitric acid to create the metallic Ir surfaces.

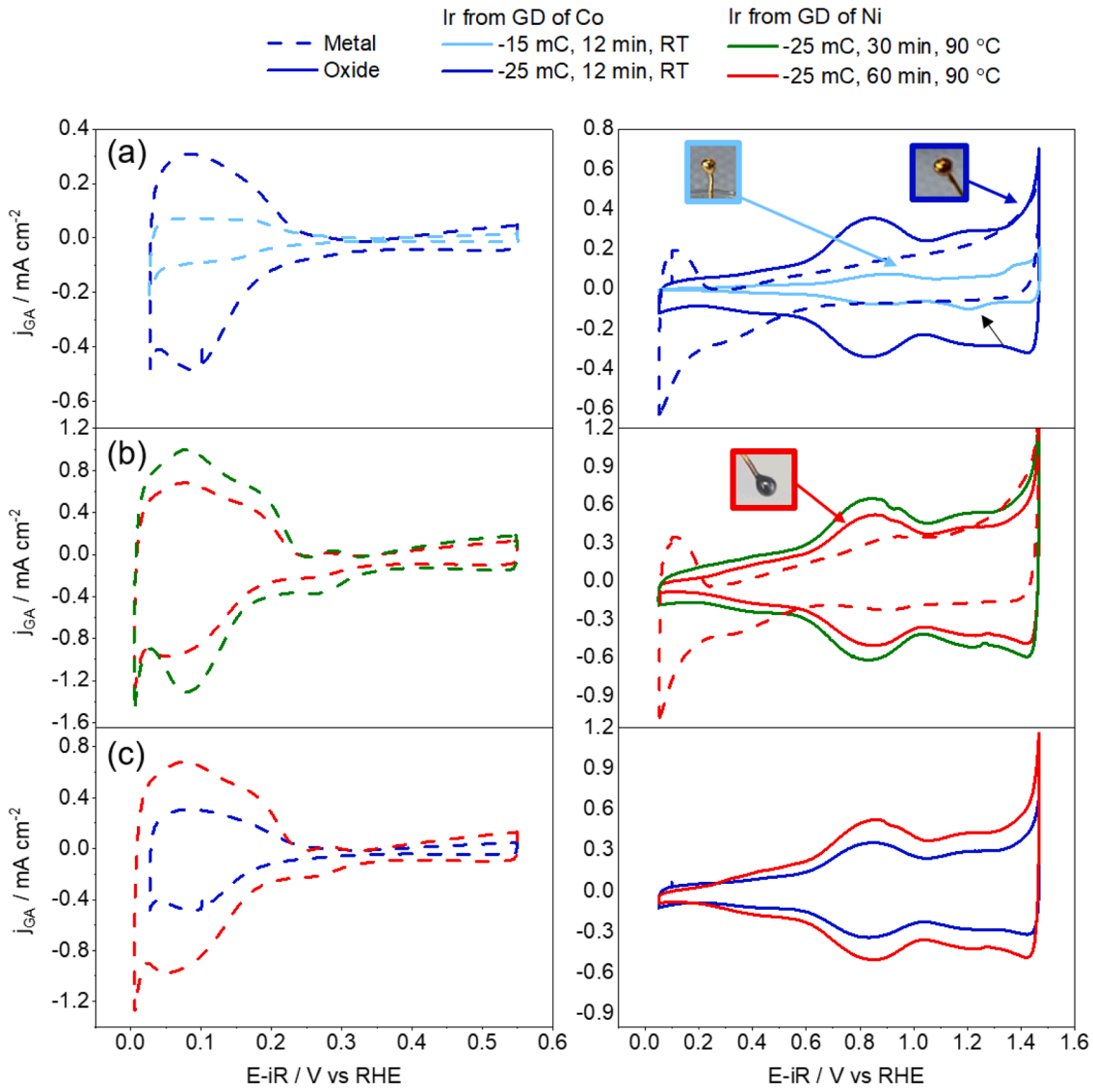

Fig. 2. Cyclic voltammograms of the metallic Ir catalysts and the conditioned IrO_2 catalysts recorded at $\nu = 50$ mV/s in 0.1 M $HClO_4$. Left: Hydrogen underpotential region of the as prepared metallic Ir surfaces between 0.0 and 0.55 V vs RHE. Right: electrochemically conditioned Ir oxides surfaces compared to the as prepared metallic surfaces between 0.05 and 1.47 V vs RHE. Different conditions of galvanic displacement were applied (referred to in the legends): (a) Shows the influence of different loadings of Co. The insets show the colours of the beads after displacement of different Co loadings. The black arrow indicates the appearance of the gold reduction peak. (b) Galvanic displacement at 90 °C and at different times for Ni displacement. The inset shows the colour on the bead after 60 min immersion. (c) Comparison between two catalysts with galvanically displaced Co (GDR at RT and for 12 min) and Ni (GDR at 90 °C and for 60 min).

(dashed lines) show prominent features between 0.0 V and 0.35 V vs RHE, which correspond to the adsorption/desorption of hydrogen, or hydrogen underpotential deposition (HUPD), on Ir [20,42,43]. These peaks are more intense as more Co is replaced, showing a correlation between the amount of Co and the amount of Ir displacing the Co. To estimate the electroactive surface area (ECSA) we integrated the charge under the HUPD voltammetric region as explained in the experimental section. We used the ECSA and GA of the beads to determine the roughness factors, R_F, of the samples (S.I. section S1). We could not estimate the ECSA of the derived Ir oxide films (IrO_2) films since hydrogen adsorption only occurs on the metallic surface [40,41,44]. Thus, we have assumed that the differences in real surface area of the respective IrO_2 layers are relative to the differences in active surface area of the metallic Ir phase and can be compared.

The ECSA of Ir prepared with Co deposited at circulated charges between −10 mC and −15 mC was similar. Its determination was difficult due to the low intensity of the recorded Ir voltammetric peaks (Fig. 2*a*, light blue line). We obtained roughness factors around 1 for the deposits prepared with deposited Co at charges between −10 mC and −15 mC. In contrast, Ir films prepared from Co deposits at −25 mC (Fig. 2*a*, dark blue dashed line) presented high roughness factors of 6.0 ± 1.3, showing that −25 mC is the optimal deposition charge for efficient GDR of Co. We also performed GDR of a −25 mC deposited Co film for 90 min (Figures S3*a* and *b*) and we do not observe a significant increase in current of the HUPD features, concluding that at 12 min the GDR of Co by Ir has been mostly completed. The formation of the corresponding IrO_2 prepared from GDR of Co is shown in the right side in Fig. 2*a* (blue solid lines). After electrochemical conditioning, the hydrogen adsorption and desorption peaks have disappeared (solid lines). We would like to note that the HUPD areas of the metallic surfaces in the right panel have already been reduced in relation to the left panels. The CVs in the right panel are recorded by going to the higher potential limit of 1.47 V vs RHE, where the metal is already oxidised before recording the hydrogen adsorption. Furthermore, the Ir(III)/Ir(IV) redox peaks at about 0.85 V vs RHE and the Ir(IV)/Ir(V) peaks at 1.2 V vs RHE become more prominent during the oxidising step. As

occurred with the voltammetric features of metallic Ir (dashed lines), the IrO_2 redox peaks are visible and more prominent for higher integrated charges (−25 mC of Co circulated charge). The capacitive current is thus shown to be correlated with the circulated charge of Co. The black arrow on the right-side panel indicates the gold reduction peak, which is visible in the CVs from GDR of Co with lower charges. The appearance of this peak is due to a low coverage of Ir on the gold surface, i.e., at −10 mC and −15 mC the gold surface remains partially uncovered. Therefore, the threshold for the circulated charge, when we deposited either Co or Ni, was chosen to be −25 mC.

We have highlighted the influence of temperature and time on the GDR of Ni in Figure S3*c*. We found the GDR at RT and 5 min immersion (Figure S3*c*, yellow line) to be very inefficient, and the blank CV of IrO_2 shows only faint IrO_2 redox peaks as well as the presence of the gold reduction peak at 1.2 V vs RHE. With further increased temperature, the efficiency of the galvanic displacement of Ni increased as seen when comparing the 60 min immersion at 65 °C (Figure S3*c*, orange line), at 75 °C (Figure S3*c*, pink line) and at 90 °C (Figure S3*c*, red line). Fig. 2b shows two different CVs for metallic Ir prepared by GDR of Ni (dashed lines) and IrO_2 after electrochemical oxidation prepared by GDR of Ni (solid lines). When the temperature of the $IrCl_4$ solution is 90 °C, and the GDR is performed with 30–60 min immersion, we observed the formation of metallic Ir (Fig. 2b, left), with prominent voltammetric features of similar intensity between 0.0 V and 0.4 V vs RHE. This result confirms that, under the selected GDR conditions, Ir from $IrCl_4$ replaces Ni and forms a metallic thin film. The derived IrO_2 from GDR of Ni appears in Fig. 2b, right panel (solid lines). The IrO_2 prepared at 30 min (yellow line) is slightly more intense than the one prepared at 60 min (red line), a fact that we ascribe to a small difference in area of the employed bead-substrates, as we melt a gold wire to grow the bead geometry (see experimental section). We conclude that the formation of IrO_2 films prepared by GDR of Ni, in the time window between 30 and 60 min, is optimal. We calculated an R_F of 15.7 ± 5.5 for Ir—Ni, i.e., about 2–3 times higher than the Ir films prepared by GDR of Co. Fig. 2*c* compares the cyclic voltammograms of the metallic and oxide Ir catalysts prepared by GDR of Co and Ni deposited at −25 mC between 0.00 and 1.47 V vs RHE. The CV in the HUPD region of the metallic Ir catalyst prepared by GDR of Ni during 60 min immersion at 90 °C has more pronounced hydrogen adsorption/desorption peaks than the metallic Ir catalyst prepared by GDR of Co during 12 min at RT. Similarly, the corresponding IrO_2 prepared from Ni has more pronounced redox peaks, clearly showing that GDR of Ni at 90 °C and 60 min generates Ir catalysts with higher active surface area and higher capacitive current.

To further investigate the nature of the IrO_2 catalysts and determine which parameters influence the catalyst surface structure, we examined the morphologies of the surfaces with SEM. We assessed the morphology of the electrodeposited Co and Ni films, as well as the derived IrO_2 films prepared by GDR, by depositing Co and Ni on the *Si/Ti/Au* surfaces, and subsequent electrochemical oxidising. Fig. 3a and b compare the Co and Ni deposits before GDR prepared by deposition in DES. The Co deposit in Fig. 3*a*, obtained at −0.75 V vs Ag and under 155 mC / cm^2 circulated charge, is comparable to the results of Landa-Castro et al on polycrystalline gold [30,45], and shows an interwoven morphology. In contrast, the Ni deposit (Fig. 3b), prepared at −0.65 V vs Ag and under 155 mC/cm^2 circulated charge, show small rounded nanoparticles, similar to previous results obtained on glassy carbon and platinum substrates [31]. We also observe the formation of big clusters in Fig. 3b, which could indicate that the Ni nanoparticles diffuse on the gold surface and agglomerate. The EDX analysis in Figure S4*a* and *b* confirmed the presence of Ni and Co on the gold substrates.

Fig. 3c and *d* compare the prepared IrO_2 surfaces after GDR of Co and Ni, leaching and subsequent electrochemical conditioning of the metallic Ir. Fig. 3c shows the SEM images of an IrO_2 catalyst prepared from GDR of Co and Fig. 3d shows the SEM images of an IrO_2 catalyst prepared from GDR of Ni on the *Si/Ti/Au* surfaces. The morphology of the derived IrO_2 deposits is different from the morphology of the Co and Ni metallic deposits. Fig. 3*c* shows that the interwoven Co morphology has disappeared and rounded nanoparticles of IrO_2 are formed. Fig. 3d highlights some additional features in the IrO_2 prepared by galvanic displacement of Ni at 90 °C. Although IrO_2 derived from Ni similarly develops nanoparticles, it additionally exhibits some holes and a more porous structure. We have also observed that the Ir—*Si/Ti/Au*, after galvanic displacement of Ni had a grey colour and was distinctly darker than the red-golden colour after displacement of Co (insets in Fig. 3c and d). The morphological features on the IrO_2 surface prepared by GD of Ni can possibly be attributed to the additional step of heating during the galvanic displacement. In combination with SEM imaging, we investigated the composition of the surfaces with EDX analysis, which is shown

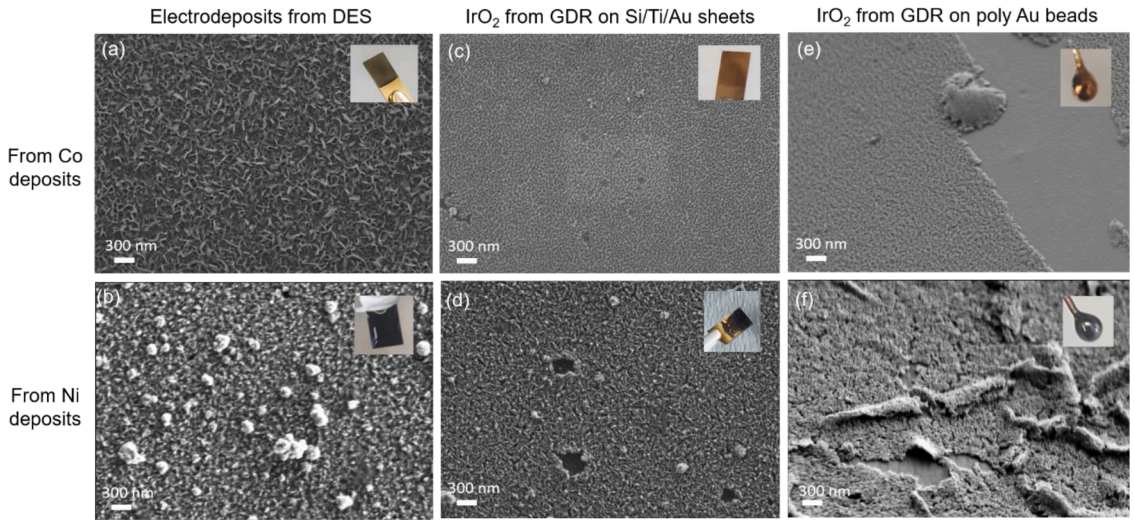

Fig. 3. Morphological analysis with field emission scanning electron microscopy. Insets show pictures of the surfaces with deposits. (a) Co electrodeposited on a Si/Ti/Au sheet in deep eutectic solvent at −0.75 V and 155 mC/cm^2 circulated charge, (b) Ni electrodeposited on a Si/Ti/Au sheet in deep eutectic solvent at −0.65 V and 155 mC/cm^2 circulated charge, (c) IrO_2 catalyst prepared by galvanic displacement of Co deposit on a polycrystalline gold bead by Ir via immersion in $IrCl_4$ for 12 min at RT and subsequent electrochemical oxidizing,(d) IrO_2 catalyst prepared by galvanic displacement of Ni deposit on a polycrystalline gold bead by Ir via immersion in $IrCl_4$ for 30 min at 90 °C and subsequent electrochemical oxidizing, (e) IrO_2 catalyst prepared by galvanic displacement of Co deposit on a Si/Ti/Au sheet by Ir via immersion in $IrCl_4$ for 12 min at RT and subsequent electrochemical oxidizing and (f) IrO_2 catalyst prepared by galvanic displacement of Ni deposit on a Si/Ti/Au sheet by Ir via immersion in $IrCl_4$ for 30 min at 90 °C and subsequent electrochemical oxidizing. All images were taken at 2 keV.

in Figure S4. The metallic Co and Ni typically dissolves when exposed to acidic media [46,47]. EDX results show that most of the Co and Ni has been eliminated during the GDR and acid leaching steps as only small or no traces of Ni and Co were detected in the EDX (Figure S4*c* and *e*). However, we observed a higher amount of Ni than Co in some spots even after leaching (Figure S4*e*). Therefore, we suspect that some Ni which was not displaced by Ir was left under the Ir surface after galvanic displacement and thus was not leached even during the long stability measurement. There was no presence of Ni in the ICP-MS analysis.

Fig. 3e and f show the SEM images of IrO_2 deposits prepared by GD of Co or Ni deposited on a gold bead. Fig. 3e shows rounded nanoparticles, similar to the morphology of IrO_2 from Co observed on the sheet. Fig. 3f shows that the morphology of IrO_2 prepared by GD of Ni contains features, which are more visible on the gold bead substrate than on the planar *Si/Ti/Au* sheets. The morphology of IrO_2 from Ni shows more porosity or roughness than the morphology of IrO_2 from Co composed of uniformly distributed rounded nanoparticles. It is worth commenting that the SEM images in Fig. 3e and f lose a bit of resolution, compared to Fig. 3c and d, likely because the curvature of the gold bead affects the SEM measurement. As in Fig. 3d, we ascribe the morphological change and the scratched surface on IrO_2 from Ni to the heating step in the GDR. We cannot discard that the different geometry or surface structure of the gold bead, can also influence the morphology of IrO_2 from Ni, compared to the *Si/Ti/Au* sheets, as the electrodeposition is structure sensitive. Overall, we show that our methodology allows for the preparation of IrO_2 thin films on substrates with different shape and structure, by carrying out Co and Ni electrodeposition followed by GDR by Ir(IV).

We performed ICP-MS measurements of the digested Ir catalysts after electrochemical tests to evaluate the GDR efficiency when either Co or Ni were replaced by Ir(IV) since the presence of oxidized surface Ni and Co can affect the replacement yield of Co and Ni. The average of the mass of Ir calculated from ICP-MS for the IrO_2 samples prepared with a circulated charge of Co of −25 mC was 10.6 ± 2 μg. This value is lower than the calculated value of 12.4 μg for a 100% efficient GDR process, i.e., the efficiency of the Co displacement is around 85%. The average mass of Ir from the IrO_2 samples prepared with Ni deposits of −25 mC was 16.4 ± 3 μg, slightly higher than the expected value of 12.4 μg. We ascribe the excess amount of Ir on the Ni-displaced catalysts to the formation of a small IrO_2 precipitate during the GDR at an increased temperature that then adheres to the surface. To check this hypothesis, we performed experiments where we immersed a blank gold bead in $IrCl_4$ solution at 90 °C for 30 to 60 min to evaluate the formation of the precipitate and its influence on the electrochemical measurements. Section S5 and Figure S5 show the electrochemical investigation of the precipitate. Figure S5*a* shows the blank CV of the blank gold bead after immersion for 60 min (first cycle) compared to the IrO_2 catalyst where the Ir has replaced electrodeposited Ni (after electrochemical oxidizing). The absence of the hydrogen peaks suggests that the precipitate is not metallic in nature. Furthermore, the peaks are less pronounced for the precipitate in relation to the Ir oxide formed by galvanic displacement and electrochemical conditioning. No traces of Co and Ni were detected in the ICP-MS analysis after sample dissolution, supporting that most of the Co or Ni is GDR replaced and/or leached out.

3.2. Activity of the IrO_2 catalysts

To evaluate the catalyst performance of the nanostructured IrO_2 catalysts towards the OER under acidic conditions we carried out cyclic voltammetry between 1.2 and 1.6 V vs RHE in 0.1 M $HClO_4$ at a scan rate of 10 mV/s (Fig. 4). We selected the 0.1 M $HClO_4$ electrolyte for the

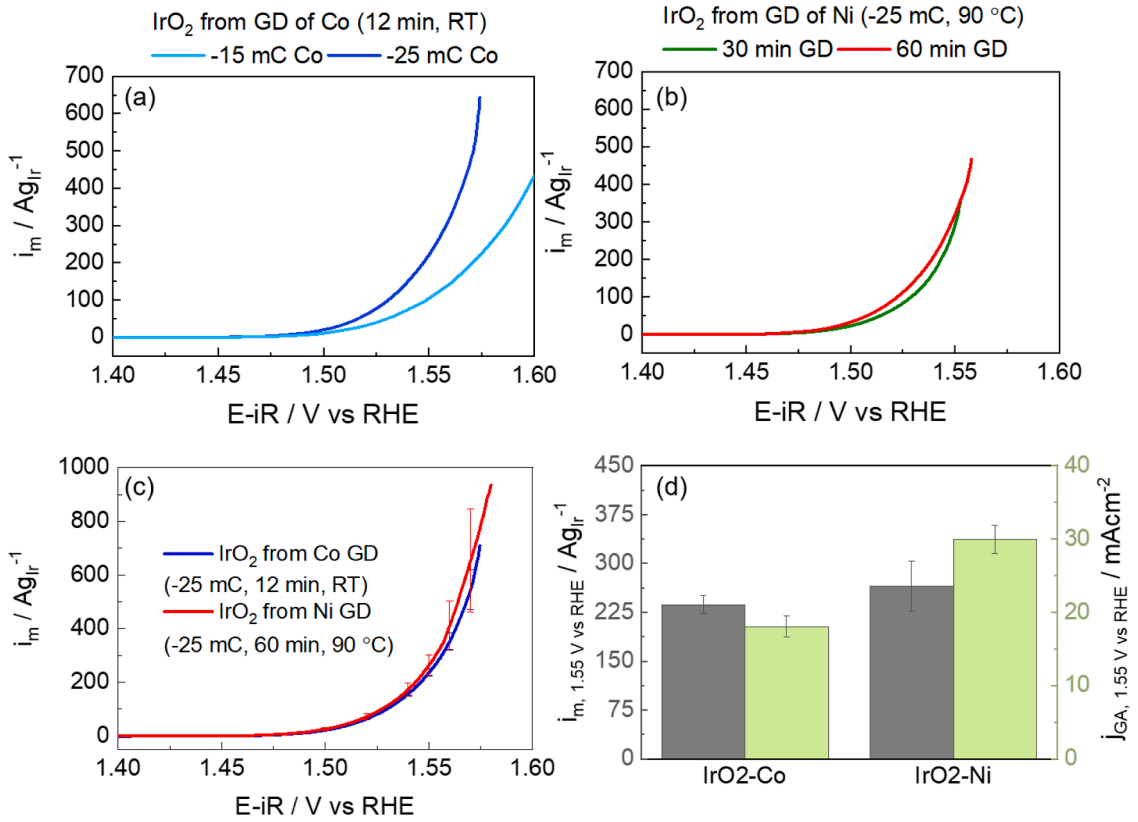

Fig. 4. IrO_2 catalyst activities at the OER. (a) Cyclic voltammogram at the OER for IrO_2 prepared by galvanic displacement of Co from different mass loadings of Co determined by the charge of −15 mC and −25 mC, respectively. (b) Cyclic voltammogram at the OER for IrO_2 prepared by galvanic displacement of Ni for different times of 30 and 60 min during galvanic displacement. (c) Cyclic voltammogram at the OER for IrO_2 at Co circulated charge of −25 mC and IrO_2 (from Ni) after 60 min galvanic displacement. All CVs were recorded at $\nu = 10$ mV/s in 0.1 M $HClO_4$. Mass activities were calculated based on the Ir mass from ICP-MS analysis after Ir dissolution. (d) Comparison of the mass activity as well as current density at 1.55 V vs RHE between the catalysts.

analysis of the OER performance, as this electrolyte does not block the surface actives sites for the OER reaction. Recently, Arminio *et al.* reported on the electrolyte effect on the OER performance on Ir black nanoparticles, finding that sulfuric acid considerably inhibited the OER due to surface poisoning by the electrolyte [48].

We prepared our catalysts and performed OER on gold beads for the following reasons: i) Au is more resistant to corrosion under anodic potentials compared to carbon supports [49–51], ii) the interconnection of Ir and Au as well as lower passivation than other supports could increase the OER stability according to previous works [51] and iii) the bead geometry facilitated the dispersion of the formed oxygen bubbles at the surface as observed during the experiments. In the long term, gold is not sustainable to use as support because of its high cost. However, it is desirable for fast screening of the electrocatalyst performance by means of cyclic voltammetry at a lab scale due to the above reasons. The stability and corrosion of the substrate are especially important to consider when applying a high potential in acid media. Previous reports on the dissolution of Ir nanoparticles during OER in relation to different substrates found that a material such as glassy carbon passivates easily on the surface, which influences the stability measurements so that the stability of the actual catalyst is difficult to determine [51]. Gold supports have previously been shown to enhance activity in alkaline media by interacting with the catalyst and changing the electronic structure and thereby the catalytic performance at active sites [52–54]. However, we observed i) that the activity of gold contributed very little to the activity of the catalysts in comparison to the activity of Ir as seen in Figure S6, and ii) that the roughness factor of the prepared Ir on gold beads was much higher than for pure gold with a roughness factor of 1. In this work, our aim is to compare OER activity and stability of the different nanostructured catalysts (rather than to investigate the effect of Au), which we prepare on Au beads due to the above reasons.

Fig. 4 reports the averages between the anodic and cathodic curves of the OER cyclic voltammograms from the same catalysts as shown in Fig. 2. Fig. 4a shows the Ir mass activity (Ag_{Ir}^{-1}) for OER of IrO_2 catalysts with two different circulated charges during Co deposition (−15 mC and −25 mC, respectively). The mass activities were calculated from the mass of Ir determined by the ICP-MS. An increase in integrated charge during the deposition results in an increase in mass activity. The increase in mass activity is related to the differences in the electroactive surface area of the Ir films deposited at different GDR conditions as seen in Fig. 2a. Figure S7*a* shows the OER activity of the two IrO_2 prepared at different circulated charges of Co normalized by the geometric area of the gold substrate. The IrO_2 nanoparticles from GD of deposited Co prepared from −25 mC have an OER geometric activity which is similar to Ir black [48]. Figs. 4b and S7b show the Ir mass activity (Ag_{Ir}^{-1}) and geometric activity for OER, respectively, of the IrO_2 catalysts prepared from GDR of Ni with immersion times of 30 min and 60 min. They are very similar in activity. This result supports that times between 30 and 60 min are optimal to prepare active IrO_2 catalysts for OER from GD of Ni. Figs. 4c and S7c show the OER activities of the IrO_2 catalyst prepared by GDR of Co (−25 mC, 12 min, RT) and of the IrO_2 catalyst prepared by GDR of Ni (−25 mC, 60 min., 90 °C). The geometric activity of the IrO_2 prepared by GD of Ni clearly surpasses the geometric activity of the IrO_2 catalyst prepared by GD of Co. Comparing the two catalyst types, the mass activities are shown to be more similar due to the increased mass of Ir oxide on the IrO_2 catalysts prepared by GD of Ni. As mentioned, the GDR efficiency found from ICP-MS was around 85% for the Co displacement but seemed to be more than 100% for the Ni displacement due to Ir precipitating on the surface during the heating step (Figure S5b). The ECSA normalised activities are shown in Figure S7*d* and appear to be more similar than the geometric and mass activities. The similarity indicates that the intrinsic activity is essentially the same for the two catalysts but due to the increased roughness of the catalysts prepared by GD of Ni, the geometric activity and mass activity are not the same. The fact that all the IrO_2 thin films show similar current densities normalized by ECSA (figure S7d) would support that neither Co or Ni are present or contribute to the intrinsic OER performance.

In Fig. 4d, the catalyst mass and geometric activities at 1.55 V vs RHE are reported for both IrO_2 prepared by GD of Co and Ni. The mass activity is shown as the grey boxes on the left side and the geometric activity is shown as the green boxes on the right side. IrO_2 catalyst prepared from a circulated charge of Co of −25 mC has a mass activity of 237 ± 14 Ag_{Ir}^{-1} (and geometric activity of 18.1 ± 1.5 $mAcm^{-2}$) at 1.55 V vs RHE. Our IrO_2 catalyst prepared by GD of Ni shows a mass activity of 265 ± 38 Ag_{Ir}^{-1} and enhanced geometric activity of 29.4 ± 2 mA cm^{-2} at 1.55 V vs RHE. We ascribe the enhancement of geometric activity to an increase of the surface area of the IrO_2 prepared by GDR of Ni due to a change in the surface morphology, induced by the different time and heating conditions during GDR (Figs. 2 and 3). Alia *et al.* found that their Ir—Ni nanowires prepared by GD of Ni by Ir had higher activity towards the OER than the similarly prepared Ir—Co nanowires, a fact that they attributed to differences in the Ni and Co morphology or presence of oxides on Ni that affected the GDR displacement rates [24].

3.3. Stability of the IrO_2 catalysts

The stability of the prepared catalysts under OER conditions were tested under both chronoamperometric and chronopotentiometric conditions. Establishing a standardized protocol to evaluate OER stability continues to be a detailed point of discussion in the field [51,55]. Different factors can affect OER stability including; i) catalyst degradation and dissolution over time, ii) weak interactions of the IrO_2 layer with the substrate, or corrosion and passivation of the substrate which can conceal the real degradation of the catalyst as described by Geiger et al [51] and iii) blockage of the active sites due to formation of oxygen micro bubbles, which increases the applied potential and accelerates the dissolution of the catalyst [55,56]. To investigate the stability of our prepared IrO_2 catalysts we performed the stability tests, i.e. chronoamperometry and chronopotentiometry measurements, at similar conditions to what has been reported in previous works [20,48].

We carried out the chronoamperometric (CA) tests for 14 h at a constant potential of 1.6 V vs RHE, with the coated gold beads immersed in the electrolyte, and without using rotating disk electrode. Previous reports have performed CA tests between 1.55 V and 1.6 V vs RHE [20, 23]. Our aim is to assess how applied constant potential affects the catalyst degradability at current densities ca. of 11–14 mA cm^{-2}. Fig. 5*a* shows the chronoamperometry transients at 1.6 V recorded for IrO_2 catalysts from GD of Co and Ni deposits of −25 mC, respectively. The chronoamperometric transients recorded for the two catalysts present similar profiles. During the first minutes, the activity shows a fast decrease of about 50% of the initial current density. After that, the activity decays slowly, although a current plateau is not reached after 14 h. The difference in activity between the catalysts prepared from Ni and Co deposits remains constant, with IrO_2 prepared from GD of Ni being more active (Fig. 5*a*, red line), in agreement with the results shown in Fig. 4*c*. The chronoamperometric transients show analogous behaviour to other transients recorded on planar electrodes in rotating disk electrode configurations previously reported [48]. Fig. 5b shows the OER activities of the IrO_2 catalysts at 10 mV/s, before and after the 14 h chronoamperometric tests at 1.6 V. We observe that the loss in activity is similar for both IrO_2 catalysts prepared from Ni and Co. For clarity, in Fig. 5*c* the mass activities are plotted for both catalysts at 1.55 V vs RHE before and after the stability. The catalyst loss in activity after the chronoamperometric test is similar on the Ni and Co displaced catalysts. This result suggests that the degradation kinetics of both IrO_2 structures are dependant on the applied potential and independent on the replaced metal (Co, Ni) during GDR.

We performed the chronopotentiometric (CP) tests by holding a constant current density of 11–14 $mAcm^2$ until dissolution of the IrO_2 catalyst. Fig. 6a shows the chronopotentiometric stability of the following IrO_2 deposits: IrO_2 prepared by GDR of deposited Co with −10 mC circulated charge, with GD at room temperature during 6 min, IrO_2

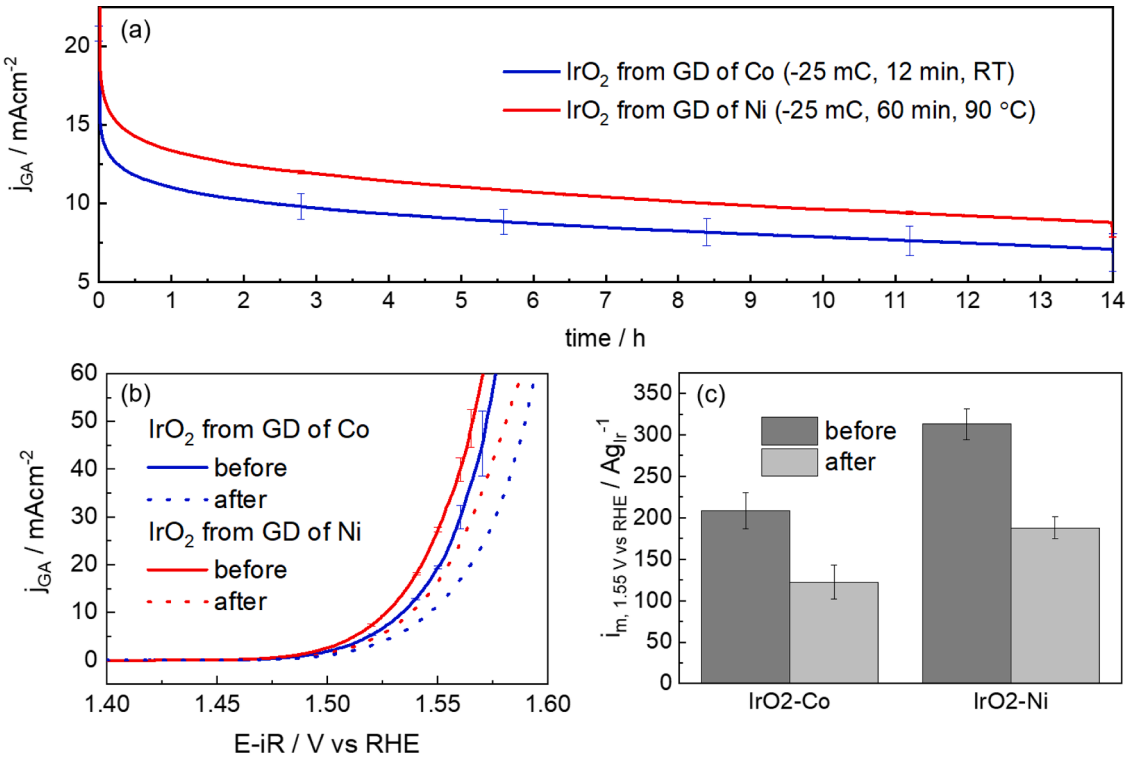

Fig. 5. Chronoamperometric stability tests for IrO_2 catalysts. All stability tests were done in 0.1 M $HClO_4$. (a) Current density activities of IrO_2 from GD of Co (conditions during GDR: −25 mC Co, 12 min immersion, room temperature) and IrO_2 from GD of Ni (conditions during GDR: −25 mC Ni, 60 min immersion, 90 °C) over 14 h of constant potential of 1.6 V. Performed at constant Ar flow. (b) OER current density activities before and after the chronoamperometric stability tests. (c) Mass activities determined from the dissolution of Ir before and after the chronoamperometric stability tests.

(−10 mC, 6 min, RT); IrO_2 prepared by GDR of deposited Co with −25 mC circulated charge, with GD at room temperature during 12 min, IrO_2 (−25mC, 12 min, RT); and IrO_2 prepared by GDR of deposited Ni with circulated charge of −25 mC, with GD at 90 °C and during 60 min, IrO_2 (−25 mC, 60 min, 90 °C). All profiles follow the same trend: The overpotential increases slowly until reaching a critical potential around 1.65 V vs RHE, at which time the rate of dissolution rapidly increases reaching the threshold potential of 2.1 V vs RHE. This potential corresponds to OER on the gold substrate, i.e., when all Ir catalyst has dissolved. The increase in the degradation kinetics as the overpotential increases can be seen as a "snowball effect" [48]. The IrO_2 catalyst with a circulated charge of Co at −10 mC and Ir loading of 33 μg/cm^2 dissolves after approximately 6 h (light blue line), whereas the IrO_2 catalyst with a circulated charge of Co at −25 mC and mass loading of 75 μg/cm^2 dissolves after approximately 26.5 h (dark blue line). Interestingly, even though both catalysts prepared from GD of Co and Ni show high chronopotentiometric stability, the IrO_2 catalyst with a circulated charge of Ni at −25 mC and mass loading of 102 μg/cm^2 is considerably more stable (red line), and did not dissolve completely after 138 h, as shown in the inset of Fig. 6a. Notably, Fig. 6a also shows that the IrO_2prepared by GD of Co (−10 mC) presents the higher initial potential, where the plateau starts, (1.58 V vs RHE), followed by IrO_2 prepared by GD of Co (−25 mC) (1.56 V vs RHE) and IrO_2 prepared by GD of Ni (1.54 V vs RHE). The correlation between the stability of the catalysts and this initial potential indicate, that the initial potential as well as the potential plateau before the complete dissolution, could have an influence on the dissolution rate of the catalyst.

Fig. 6b shows the CVs of the two catalysts prepared from −25 mC deposits just before the stability test. We observed that the potential difference between the samples, at currents between 11 and 14 mA cm^{-2} is consistent with the difference in initial potential in the chronopotentiometry experiments. Fig. 6b also shows the CVs in the OER region for each prepared catalyst after the stability test. The CV of IrO_2 prepared from GD of Co do not show activity after the stability test and is similar to that of polycrystalline gold, confirming the full dissolution of the catalyst. In contrast, the CV of IrO_2 prepared from GD of Ni after the stability test still shows OER activity indicating that the catalyst did not fully dissolve after operating for 5 days, which is also evident by the lack of potential jump in the curve in Fig. 6a. However, the activity has considerably decreased as seen in the red dashed line in Fig. 6b. Interestingly, the potential value in the CV at which 12.5 mAcm^2 is reached after 138 h of testing (1.60 V vs RHE), is approaching the potential value of the chronopotentiometry at this time (1.66 V vs RHE).

To assess the stability of our prepared samples under a constant OER applied current, we have evaluated the total charge (Q_{OER}) from the applied current ($I_{applied}$) and time of dissolution (t_{dis}) during the CP stability tests as a function of the Ir loading (m_{Ir}) determined by ICP-MS. We then approximately determined the stability number, S, introduced by Geiger et al [57] as moles of generated oxygen per mole of Ir: n_{O2}/n_{Ir} using Faraday's law so that:

$$S = n_{O2}/n_{Ir} = I_{applied} * t_{dis} * M_{Ir}/nFm_{Ir}$$

Where M_{Ir} is the molar mass of Ir (192 g/mol) and n is the number of electrons transferred during OER. By coupling a scanning flow cell (SFC) to an ICP-MS, Geiger et al. were able to determine the amount of dissolved Ir in situ. The detection of Ir was carried out during a short potential sweep and at different constant currents for a given Ir loading. Our *S*-numbers are affected by the fact that Ir dissolves over time, changing the needed potential to maintain a constant current density, which increases the mass activity and rate dissolution over time. For the IrO_2 catalyst prepared from GD of Co, −10 mC in Fig. 6a, with a loading of 33 μg_{Ir} cm^{-2} the total OER charge was 50 C, i.e., the *S*-number was 0.5×10^4. For a loading of 72 μg_{Ir} cm^{-2} in IrO_2, prepared by circulated charge of −25 mC Co, the *S*-number was 0.9×10^4 (charge of 191 C). For a loading of 102 μg_{Ir} cm^{-2} for IrO_2 prepared by Ni, −25 mC, the *S*-

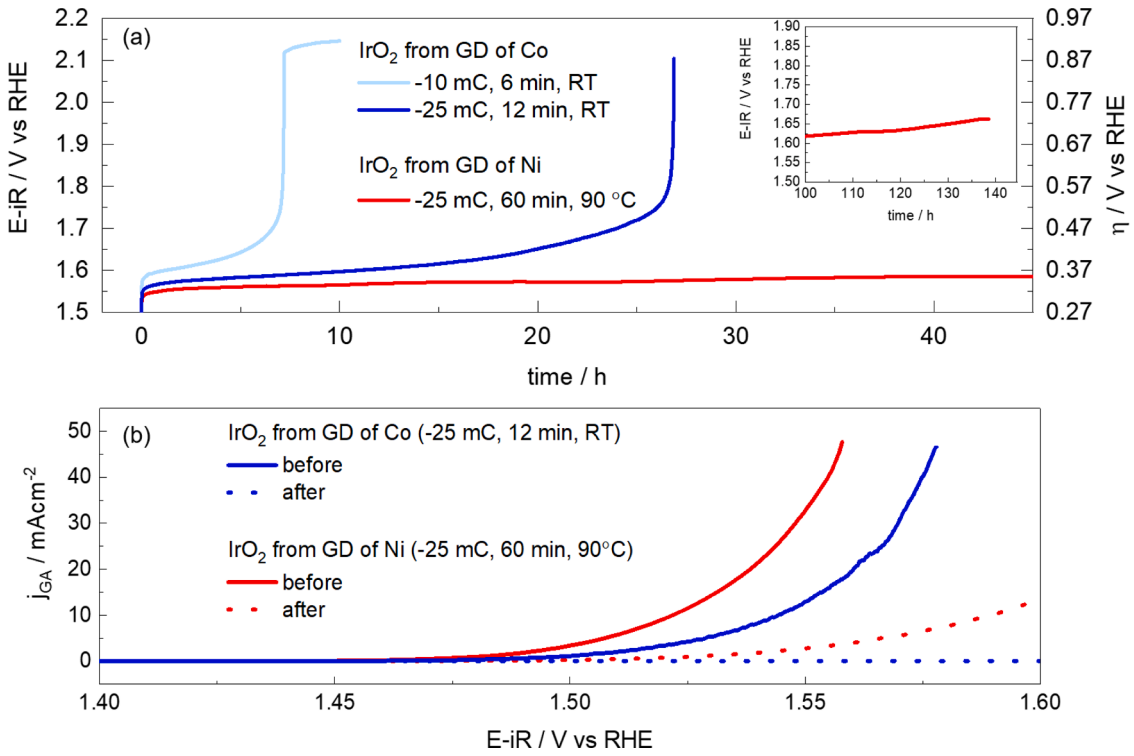

Fig. 6. Chronopotentiometric stability for IrO_2 catalysts at a constant current. All tests were done in 0.1 M $HClO_4$. (a) Potential (left axis) and overpotential (right axis) of IrO_2 prepared from GD of different loadings of Co (light and dark blue lines) with GD at room temperature and IrO_2 prepared from −25 mC circulated charge of Ni by GD at 60 min and 90 °C (red line) during stability tests at constant current densities of 11–14 mA/cm^2. (b) OER current density activity before (solid lines) and after (dashed lines) the stability measurements of IrO_2 prepared from a −25 mC loading of Co with GD at room temperature (dark blue) and IrO_2 prepared from a −25 mC loading of Ni with GD at 60 min immersion at 90 °C (red line). The loading of the samples, determined by ICP after fully dissolving the Ir, are: 33 μg_{Ir} cm^{-2} in IrO_2 from Co (−10 mC), 75 μg_{Ir} cm^{-2} in IrO_2 from Co (−25 mC), and 102 μg_{Ir} cm^{-2} in IrO_2 from Ni (−25 mC).

number was higher than 3×10^4 (charge higher than 994 C). The results show that the IrO_2 system prepared by GD of Ni is considerably more stable than IrO_2 prepared by GD of Co at the same applied constant OER current. The *S*-number of the highly stable IrO_2–Ni is similar to that of hydrous IrO_x reported by Geiger et al. However, to fully compare the values, an in situ study of our catalyst degradation would be preferred. The increase in the *S*-numbers, in the order IrO_2–Ni, −25 mC > IrO_2–Co, −25mC > IrO_2–Co, −10 mC, is too significant to be only affected by differences in the Ir loading between samples. We ascribe these results to the fact that IrO_2 prepared by GD of Ni has the highest active surface area among our prepared catalysts, and therefore less applied potential is needed to achieve the same current density (Fig. 6). Thus, tuning the surface structure is key to decrease the onset potential, perform OER at high rates and reduce the IrO_2 corrosion rate [48]. We also observed that the Ir precipitate, which contributed to the increased mass on the IrO_2 prepared by GD of Ni beads, did not show a high stability in relation to the Ir displaced from Ni. Figure S5*c* shows the stability during CP of a blank gold bead immersed in $IrCl_4$ for 60 min, which is negligible in relation to the high stability of the IrO_2 catalyst prepared by GD of Ni seen in Fig. 6.

3.4. Discussion

IrO_2 anodes on proton exchange membrane electrolysers show two to three orders of magnitude higher stability than that of our prepared materials and can operate at high current densities for several years [57,58] which means that the stability of our materials is likely to be underestimated. The dissolution of a catalyst in an electrochemical cell using a thin layer of catalyst differs from that of an industrial PEM electrolyser. Thus, the stability measurements can mainly be compared internally with other laboratory experiments in three-electrode cells and under potential control conditions. Our measurements in a conventional three-electrode cell are likely influenced by the formation of microbubbles of oxygen that block active sites, increase the applied potential and accelerate the degradation [59]. We do not discard that the more porous IrO_2 morphology when preparing the catalysts from Ni GD, in Fig. 2*d* can disperse the micro-oxygen bubbles better than the morphology of the IrO_2 prepared from GD of Co and thereby increase the catalyst stability [60,61].

Several groups have previously investigated the OER in acidic media on Ir—based catalysts, some doped with other metals such as Ni or Co, and reported mass activities between 600 and 2000 $A g_{Ir}^{-1}$ at 1.55 V vs RHE using the rotating disk electrode configuration [23,47,48,62–65]. Even though our IrO_2 catalysts show lower mass activities than previously reported Ir—based catalysts, we showed that they could reach a current of 10 mA/cm^2 at a reduced overpotential of 295 ± 3 V vs RHE and operate for more than 130 h. It must be noted that leaching of the non-noble metal (Co or Ni) considerably improves the activity and stability of the IrO_2 thin films, as reported in the works by Alia et al [24] and Jensen *et al* [23] We want to highlight that direct comparison between catalysts is not always straightforward as electrochemical conditions can vary between different works such as: the selected electrolyte [48] and the type of method used to address the nanoparticles stability, which highly depends on the applied potential or constant current conditions; and the Ir mass loading and surface structure. In our work, we aimed to evaluate how these different experimental parameters influence the OER stability of our electrodeposited films.

Other setups than the three-electrode liquid cells, such as gas diffusion electrodes (GDE), are often used with the goal of simulating more realistic conditions comparable to PEMWE. GDE setups solve the problem of mass transport limitations in conventional three-electrode cells to reach high current densities for water splitting [66,67]. GDE have been

used by e.g. the Arenz group to investigate the influence of different parameters on the OER such as loadings, electrolyte temperature and substrate [68–70]. The authors have prepared nanoporous IrCo of mixed oxide with a 0.25 mg cm^{-2} loading of Ir, reaching an activity of 101.5 Ag_{Ir}^{-1} at 1.50 V vs RHE, which is within the order of magnitude of our prepared nanostructures [68]. We realise that, to test our catalysts in more realistic devices, future steps should be taken towards implementing our catalysts in a GDE setup through electrodeposition. Here, we mainly address the fundamental aspects and feasibility of the method to prepare IrO_2 films on conducive and extended surfaces with variable shape, such as bead and planar electrodes.

It is also worth mentioning that several groups are now working with dimensionally stable anodes (DSA), which are metal oxide catalysts coated on a substrate that is scalable such as Ti, Sn [14] or Ta oxides. These valve metal oxides are corrosion-resistant providing high stability to the active metal oxide [71–73]. Additionally, high mass activities are reached by using these systems. Touni *et al.* reported IrO_2/Ir—TiO_2/Ti anodes with activities of 560 Ag^{-1} at 1.60 V vs RHE [72,74]. Nanoscale DSA-like electrodes were also investigated by Zheng et al [15], where they reported mass-selected small $Ir_{0.1}Ta_{0.9}O_{2.45}$ catalysts down to 1–2 nm with mass activities of 1200 ± 0.5 A g_{Ir}^{-1} at 1.55 V vs RHE. One problem is that these metal oxides are typically semi-conductive or non-conductive, which makes it necessary to increase the IrO_2 percentage in the anode for active OER [75]. To improve the electronic conductivity across the anode layer and reduce loadings of Ir, Millet and co-workers used micro-sized metallic Ti particles coated by IrO_2 for OER in PEM electrolysers [75,76]. The prepared IrO_2/TiO_2/Ti anodes had increased electroactive surface area and showed activities of 1 A cm^{-2} for more than 6000 h. These works show that combining corrosion-resistant substrates with enough electronic conductivity, and large active surface areas of the IrO_2 catalyst are beneficial both for active and stable OER, aligning with the fundamental findings of our work on IrO_2-coated gold substrates.

Here we have presented a method that combines electrodeposition in deep eutectic solvent of Ni and Co, which are later replaced galvanically by Ir. Deep eutectic solvents have the potential to prepare materials for industry due to different benefits; they have a wide potential window, allowing for the preparation of a variety of materials by electrodeposition of different elements, such as Co and Ni, and without the problem of evolving hydrogen in aqueous solvents. Moreover, electrodeposition in DES offers additional advantages such as a more homogeneous distribution of particles with reduced amount of waste materials [34,77,78]. However, the method does present some drawbacks to overcome before further scaling, since DES have high viscosity, leading to low rates of deposition, and can degrade over time [79]. Additionally, GDR of Ni by Ir is not straightforward as it is kinetically hindered (as we needed to increase the temperature). These drawbacks may particularly limit the application of our method for the modification of the diffuse layers of GDE and MEA. Next steps should focus on implementing the use of DES at first on GDE electrodes, for example by using DES/water mixtures with reduced viscosity for better impregnation of the diffuse layer and faster deposition kinetics. In the future, we also aim to assess how modifying the parameters of the GDR, such as the amount of replaced Co or Ni, might affect the mass activities of our IrO_2 catalysts, with the aim to reduce loadings of Ir.

4. Conclusions

In this work, we highlight the galvanic displacement reaction method as a feasible method to fabricate thin nanostructured films of IrO_2 from electrodeposited Co and Ni in choline chloride urea deep eutectic solvent. We found that GDR of Ni by Ir at 90 °C for 60 min generates films with higher active surface area and higher OER geometric activity. Curiously, the IrO_2 catalysts prepared by GD of Ni show a highly enhanced stability in relation to those prepared by GD of Co. We highlight the simplicity and sustainability of this method to prepare the IrO_2 catalysts, which makes it worth pursuing. The electrodeposition technique also offers the advantage of modifying conductive surfaces with different shapes and geometries. We emphasise that the effect of substrates of different geometry and nature, the structure and roughness of the deposited IrO_2 thin films should be also considered in future works. As deposition is a surface structure sensitive processes, different substrates can influence morphology and performance of the deposited IrO_2 films. Furthermore, electrodeposition in DES to create bi- and multi-metallic structures has also been proven feasible in our recently published reports [32,80], and opens pathways to develop more sustainable routes to fabricate bimetallic Ir—based catalyst structures for the OER [12,81–83]. With our IrO_2 catalysts prepared by GD of Ni we were able to carry out OER at the same constant current density as for IrO_2 prepared from Co, but for around 10 times longer. Both IrO_2 prepared by GD of Co and Ni had the same degradation rate at constant potential, showing that the type of metal does not influence the IrO_2 dissolution mechanism for a given potential value. Differences in surface morphology induced by the heating step during the GDR of Ni influenced the active surface area and can be a reason for the enhanced stability, at constant current, of the IrO_2 films prepared from GD of Ni. The strategies presented in our work, can be relevant to tailor the surface structure and reduce loadings of Ir, key aspects for the design of more stable IrO_2 catalysts capable of reaching high activities at low potentials.

CRediT authorship contribution statement

Freja Bech Holde: Investigation, Methodology, Formal analysis, Data curation, Writing – original draft, Visualization. **Paula Sebastián-Pascual:** Supervision, Methodology, Conceptualization, Writing – original draft, Visualization, Project administration. **Kim Nicole Dalby:** Investigation, Formal analysis, Data curation, Writing – review & editing, Resources. **Elvira Gómez:** Methodology, Resources, Writing – review & editing. **María Escudero-Escribano:** Supervision, Methodology, Conceptualization, Writing – review & editing, Project administration, Funding acquisition, Resources.

Declaration of Competing Interest

The authors declare that they have no known competing financial interests or personal relationships that could have appeared to influence the work reported in this paper.

Data availability

Data will be made available on request.

Acknowledgements

M.E.E. acknowledges the Villum Foundation for financial support through a Villum Young Investigator Grant (project number: 19142). This work was also supported by the Independent Research Fund Denmark through the DFF-Research Project1 (Thematic Research, green transition) grant with number: 0217-00213A. We acknowledge support from the Danish National Research Foundation and center for High Entropy Alloy Catalysis (DNRF-149, CHEAC). We also acknowledge Theis Brock-Nannestad from the University of Copenhagen, for providing facilities and performing most of the ICP measurements of the Ir samples, and Kim Degn Jensen who measured one of the ICP samples. We also acknowledge Hanne Falsig from Topsoe AS for providing valuable discussions.

Supplementary materials

Supplementary material associated with this article can be found, in the online version, at doi:10.1016/j.electacta.2023.143058.

References

[1] P.C.K. Vesborg, T.F. Jaramillo, Addressing the terawatt challenge: scalability in the supply of chemical elements for renewable energy, RSC Adv. 2 (2012) 7933–7947, https://doi.org/10.1039/c2ra20839c.

[2] BP, BP Statistical Review of World Energy 2020, Stat. Rev. World Energy 67 (2020) 1–56. bp.com/statisticalreview.

[3] N. Abas, A. Kalair, N. Khan, Review of fossil fuels and future energy technologies, Futures 69 (2015) 31–49, https://doi.org/10.1016/j.futures.2015.03.003.

[4] J.O. Abe, A.P.I. Popoola, E. Ajenifuja, O.M. Popoola, Hydrogen energy, economy and storage: review and recommendation, Int. J. Hydrog. Energy. 44 (2019) 15072–15086, https://doi.org/10.1016/j.ijhydene.2019.04.068.

[5] I. Staffell, D. Scamman, A. Velazquez Abad, P. Balcombe, P.E. Dodds, P. Ekins, N. Shah, K.R. Ward, The role of hydrogen and fuel cells in the global energy system, Energy Environ. Sci. 12 (2019) 463–491, https://doi.org/10.1039/c8ee01157e.

[6] I. Katsounaros, S. Cherevko, A.R. Zeradjanin, K.J.J. Mayrhofer, Oxygen electrochemistry as a cornerstone for sustainable energy conversion, Angew. Chem. Int. Ed. 53 (2014) 102–121, https://doi.org/10.1002/anie.201306588.

[7] J. Kibsgaard, I. Chorkendorff, Considerations for the scaling-up of water splitting catalysts, Nat. Energy 4 (2019) 430–433, https://doi.org/10.1038/s41560-019-0407-1.

[8] K.E. Ayers, E.B. Anderson, C. Capuano, B. Carter, L. Dalton, G. Hanlon, J. Manco, M. Niedzwiecki, Research advances towards low cost, high efficiency PEM electrolysis, ECS Trans. 33 (2010) 3–15, https://doi.org/10.1149/1.3484496.

[9] J. Rossmeisl, Z.W. Qu, H. Zhu, G.J. Kroes, J.K. Nørskov, Electrolysis of water on oxide surfaces, J. Electroanal. Chem. 607 (2007) 83–89, https://doi.org/10.1016/j.jelechem.2006.11.008.

[10] T. Reier, H.N. Nong, D. Teschner, R. Schlögl, P. Strasser, Electrocatalytic oxygen evolution reaction in acidic environments – reaction mechanisms and catalysts, Adv. Energy Mater. 7 (2017), https://doi.org/10.1002/aenm.201601275.

[11] J. Song, C. Wei, Z.F. Huang, C. Liu, L. Zeng, X. Wang, Z.J. Xu, A review on fundamentals for designing oxygen evolution electrocatalysts, Chem. Soc. Rev. 49 (2020) 2196–2214, https://doi.org/10.1039/c9cs00607a.

[12] M. Escudero-Escribano, A.F. Pedersen, E.A. Paoli, R. Frydendal, D. Friebel, P. Malacrida, J. Rossmeisl, I.E.L. Stephens, I. Chorkendorff, Importance of surface IrOx in stabilizing RuO_2 for oxygen evolution, J. Phys. Chem. B 122 (2018) 947–955, https://doi.org/10.1021/acs.jpcb.7b07047.

[13] S. Cherevko, S. Geiger, O. Kasian, N. Kulyk, J.P. Grote, A. Savan, B.R. Shrestha, S. Merzlikin, B. Breitbach, A. Ludwig, K.J.J. Mayrhofer, Oxygen and hydrogen evolution reactions on Ru, RuO_2, Ir, and IrO_2 thin film electrodes in acidic and alkaline electrolytes: a comparative study on activity and stability, Catal. Today 262 (2016) 170–180, https://doi.org/10.1016/j.cattod.2015.08.014.

[14] G.C. da Silva, S.I. Venturini, S. Zhang, M. Löffler, Oxygen evolution reaction on tin oxides supported iridium catalysts: do we need dopants? ChemElectroChem (2020) 2330–2339, https://doi.org/10.1002/celc.202000391.

[15] Y. Zheng, J. Vernieres, Z. Wang, K. Zhang, D. Hochfilzer, K. Krempl, T. Liao, F. Presel, T. Altantzis, J. Fatermans, S.B. Scott, N.M. Secher, C. Moon, P. Liu, S. Bals, S. Van Aert, A. Cao, M. Anand, J.K. Nørskov, J. Kibsgaard, I. Chorkendorff, Monitoring oxygen production on mass-selected iridium-tantalum oxide electrocatalysts, Nat. Energy 7 (2022) 55–64, https://doi.org/10.1038/s41560-021-00948-w.

[16] M.A. Hubert, A. Gallo, Y. Liu, E. Valle, J. Sanchez, D. Sokaras, R. Sinclair, L. A. King, T.F. Jaramillo, Characterization of a dynamic $Y_2Ir_2O_7$ catalyst during the oxygen evolution reaction in acid, J. Phys. Chem. C 126 (2022) 1751–1760, https://doi.org/10.1021/acs.jpcc.1c07760.

[17] Y. Chen, H. Li, J. Wang, Y. Du, S. Xi, Y. Sun, M. Sherburne, J.W. Ager, A.C. Fisher, Z.J. Xu, Exceptionally active iridium evolved from a pseudo-cubic perovskite for oxygen evolution in acid, Nat. Commun. 10 (2019), https://doi.org/10.1038/s41467-019-08532-3.

[18] O. Kasian, T. Li, A.M. Mingers, K. Schweinar, A. Savan, A. Ludwig, K. Mayrhofer, Stabilization of an iridium oxygen evolution catalyst by titanium oxides, J. Phys. Energy 3 (2021), https://doi.org/10.1088/2515-7655/abbd34.

[19] D. Escalera-lópez, K.D. Jensen, N.V. Rees, M. Escudero-escribano, Electrochemically decorated iridium electrodes with WS 3 − x toward improved oxygen evolution electrocatalyst stability in acidic electrolytes, Adv. Sustain. Syst. 1–12 (2021), 2000284, https://doi.org/10.1002/adsu.202000284.

[20] J.A. Arminio-Ravelo, J. Quinson, M.A. Pedersen, J.J.K. Kirkensgaard, M. Arenz, M. Escudero-Escribano, Synthesis of iridium nanocatalysts for water oxidation in acid: effect of the surfactant, ChemCatChem. 12 (2020) 1282–1287, https://doi.org/10.1002/cctc.201902190.

[21] D. Li, C. Wang, D. Tripkovic, S. Sun, N.M. Markovic, V.R. Stamenkovic, Surfactant removal for colloidal nanoparticles from solution synthesis: the effect on catalytic performance, ACS Catal. 2 (2012) 1358–1362, https://doi.org/10.1021/cs300219j.

[22] M.A. Montiel, F.J. Vidal-Iglesias, V. Montiel, J. Solla-Gullón, Electrocatalysis on shape-controlled metal nanoparticles: progress in surface cleaning methodologies, Curr. Opin. Electrochem. 1 (2017) 34–39, https://doi.org/10.1016/j.coelec.2016.12.007.

[23] A.W. Jensen, G.W. Sievers, K.D. Jensen, J. Quinson, J.A. Arminio-Ravelo, V. Brüser, M. Arenz, M. Escudero-Escribano, Self-supported nanostructured iridium-based networks as highly active electrocatalysts for oxygen evolution in acidic media, J. Mater. Chem. A 8 (2020) 1066–1071, https://doi.org/10.1039/c9ta12796h.

[24] S.M. Alia, S. Shulda, C. Ngo, S. Pylypenko, B.S. Pivovar, Iridium-based nanowires as highly active, oxygen evolution reaction electrocatalysts, ACS Catal. 8 (2018) 2111–2120, https://doi.org/10.1021/acscatal.7b03787.

[25] S.M. Alia, Y.S. Yan, B.S. Pivovar, Galvanic displacement as a route to highly active and durable extended surface electrocatalysts, Catal. Sci. Technol. 4 (2014) 3589–3600, https://doi.org/10.1039/c4cy00736k.

[26] A. Papaderakis, I. Mintsouli, J. Georgieva, S. Sotiropoulos, Electrocatalysts prepared by galvanic replacement, Catalysts 7 (2017), https://doi.org/10.3390/catal7030080.

[27] P. Sebastián-Pascual, I. Jordão Pereira, M. Escudero-Escribano, Tailored electrocatalysts by controlled electrochemical deposition and surface nanostructuring, Chem. Commun. 56 (2020) 13261–13272, https://doi.org/10.1039/d0cc06099b.

[28] Q. Zhang, Q. Wang, S. Zhang, X. Lu, X. Zhang, Electrodeposition in ionic liquids, ChemPhysChem. 17 (2016) 335–351, https://doi.org/10.1002/cphc.201500713.

[29] A.P. Abbott, G. Capper, D.L. Davies, R.K. Rasheed, V. Tambyrajah, Novel solvent properties of choline chloride/urea mixtures, Chem. Commun. (2003) 70–71, https://doi.org/10.1039/b210714g.

[30] M. Landa-Castro, P. Sebastián, M.I. Giannotti, A. Serrà, E. Gómez, Electrodeposition of nanostructured cobalt films from a deep eutectic solvent: influence of the substrate and deposition potential range, Electrochim. Acta 359 (2020), 136928, https://doi.org/10.1016/j.electacta.2020.136928.

[31] P. Sebastian, M.I. Giannotti, E. Gómez, J.M. Feliu, Surface sensitive nickel electrodeposition in deep eutectic solvent, ACS Appl. Energy Mater. 1 (2018) 1016–1028, https://doi.org/10.1021/acsaem.7b00177.

[32] E. Plaza-Mayoral, P. Sebastián-Pascual, K.N. Dalby, K.D. Jensen, I. Chorkendorff, H. Falsig, M. Escudero-Escribano, Preparation of high surface area Cu-Au bimetallic nanostructured materials by co-electrodeposition in a deep eutectic solvent, Electrochim. Acta 398 (2021), 139309, https://doi.org/10.1016/j.electacta.2021.139309.

[33] F. Liu, Y. Deng, X. Han, W. Hu, C. Zhong, Electrodeposition of metals and alloys from ionic liquids, J. Alloys Compd. 654 (2016) 163–170, https://doi.org/10.1016/j.jallcom.2015.09.137.

[34] E.L. Smith, A.P. Abbott, K.S. Ryder, Deep eutectic solvents (DESs) and their applications, Chem. Rev. 114 (2014) 11060–11082, https://doi.org/10.1021/cr300162p.

[35] W. Schwarzacher, Electrodeposition: a technology for the future, Electrochem. Soc. Interface. 15 (2006) 32.

[36] H. Kim, N.P. Subramanian, B.N. Popov, Preparation of PEM fuel cell electrodes using pulse electrodeposition, J. Power Sources. 138 (2004) 14–24, https://doi.org/10.1016/j.jpowsour.2004.06.012.

[37] H. Kim, B.N. Popov, Development of novel method for preparation of PEMFC electrodes, Electrochem. Solid-State Lett. 7 (2004) 1–5, https://doi.org/10.1149/1.1648611.

[38] J. Clavilier, R. Faure, G. Guinet, R. Durand, Preparation of monocrystalline pt microelectrodes and electrochemical study of the plane surfaces cut in the direction of the (111) and (110) planes, J. Electroanal. Chem. Interfacial Electrochem. 107 (1980) 205–209.

[39] A.J. Bard, G. Inzelt, F. Scholz, Electrochemical Dictionary, Springer, 2008.

[40] S. Trasatti, O.A. Petrii, Real surface area measurements in electrochemistry, J. Electroanal. Chem. 144 (1996) N3–N4, https://doi.org/10.1016/0926-860x(96)80148-7.

[41] M. Lukaszewski, M. Soszko, A. Czerwiński, Electrochemical methods of real surface area determination of noble metal electrodes - an overview, Int. J. Electrochem. Sci. 11 (2016) 4442–4469, https://doi.org/10.20964/2016.06.71.

[42] T. Reier, M. Oezaslan, P. Strasser, Electrocatalytic oxygen evolution reaction (OER) on Ru, Ir, and Pt catalysts: a comparative study of nanoparticles and bulk materials, ACS Catal. 2 (2012) 1765–1772, https://doi.org/10.1021/cs3003098.

[43] B. Łosiewicz, R. Jurczakowski, A. Lasia, Kinetics of hydrogen underpotential deposition at iridium in sulfuric and perchloric acids, Electrochim. Acta 225 (2017) 160–167, https://doi.org/10.1016/j.electacta.2016.12.116.

[44] S.M. Alia, K.E. Hurst, S.S. Kocha, B.S. Pivovar, Mercury underpotential deposition to determine iridium and iridium oxide electrochemical surface areas, J. Electrochem. Soc. 163 (2016) F3051–F3056, https://doi.org/10.1149/2.0071611jes.

[45] A. Serrà, P. Sebastián-Pascual, M. Landa-Castro, E. Gómez, Electrochemical assessment of high active area of cobalt deposited in deep eutectic solvent, J. Electroanal. Chem. (2021) 896, https://doi.org/10.1016/j.jelechem.2021.115177.

[46] C. Spöri, P. Briois, H.N. Nong, T. Reier, A. Billard, S. Kühl, D. Teschner, P. Strasser, Experimental activity descriptors for iridium-based catalysts for the electrochemical oxygen evolution reaction (OER), ACS Catal. 9 (2019) 6653–6663, https://doi.org/10.1021/acscatal.9b00648.

[47] H.N. Nong, H.S. Oh, T. Reier, E. Willinger, M.G. Willinger, V. Petkov, D. Teschner, P. Strasser, Oxide-supported IrNiOx core-shell particles as efficient, cost-effective, and stable catalysts for electrochemical water splitting, Angew. Chem. Int. Ed. 54 (2015) 2975–2979, https://doi.org/10.1002/anie.201411072.

[48] J.A. Arminio-Ravelo, A.W. Jensen, K.D. Jensen, J. Quinson, M. Escudero-Escribano, Electrolyte effects on the electrocatalytic performance of iridium-based nanoparticles for oxygen evolution in rotating disc electrodes, ChemPhysChem 20 (2019) 2956–2963, https://doi.org/10.1002/cphc.201900902.

[49] S. Cherevko, A.R. Zeradjanin, A.A. Topalov, N. Kulyk, I. Katsounaros, K.J. J. Mayrhofer, Dissolution of noble metals during oxygen evolution in acidic media, ChemCatChem 6 (2014) 2219–2223, https://doi.org/10.1002/cctc.201402194.

[50] S. Cherevko, A.A. Topalov, A.R. Zeradjanin, I. Katsounaros, K.J.J. Mayrhofer, Gold dissolution: towards understanding of noble metal corrosion, RSC Adv. 3 (2013) 16516–16527, https://doi.org/10.1039/c3ra42684j.

[51] S. Geiger, O. Kasian, A.M. Mingers, S.S. Nicley, K. Haenen, K.J.J. Mayrhofer, S. Cherevko, Catalyst stability benchmarking for the oxygen evolution reaction: the

importance of backing electrode material and dissolution in accelerated aging studies, ChemSusChem 10 (2017) 4140–4143, https://doi.org/10.1002/cssc.201701523.
[52] A. Vojvodic, T.F. Jaramillo, Gold-supported cerium-doped NiO, Nature Energy (2016) 1–18, 16053.
[53] Y. Gorlin, C.J. Chung, J.D. Benck, D. Nordlund, L. Seitz, T.C. Weng, D. Sokaras, B. M. Clemens, T.F. Jaramillo, Understanding interactions between manganese oxide and gold that lead to enhanced activity for electrocatalytic water oxidation, J. Am. Chem. Soc. 136 (2014) 4920–4926, https://doi.org/10.1021/ja407581w.
[54] R. Frydendal, M. Busch, N.B. Halck, E.A. Paoli, P. Krtil, I. Chorkendorff, J. Rossmeisl, Enhancing activity for the oxygen evolution reaction: the beneficial interaction of gold with manganese and cobalt oxides, ChemCatChem 7 (2015) 149–154, https://doi.org/10.1002/cctc.201402756.
[55] K. Ehelebe, D. Escalera-López, S. Cherevko, Limitations of aqueous model systems in the stability assessment of electrocatalysts for oxygen reactions in fuel cell and electrolyzers, Curr. Opin. Electrochem. 29 (2021), 100832, https://doi.org/10.1016/j.coelec.2021.100832.
[56] H.A. El-Sayed, A. Weiß, L.F. Olbrich, G.P. Putro, H.A. Gasteiger, OER catalyst stability investigation using RDE technique: a stability measure or an artifact? J. Electrochem. Soc. 166 (2019) F458–F464, https://doi.org/10.1149/2.0301908jes.
[57] S. Geiger, O. Kasian, M. Ledendecker, E. Pizzutilo, A.M. Mingers, W.T. Fu, O. Diaz-Morales, Z. Li, T. Oellers, L. Fruchter, A. Ludwig, K.J.J. Mayrhofer, M.T.M. Koper, S. Cherevko, The stability number as a metric for electrocatalyst stability benchmarking, Nat. Catal. 1 (2018) 508–515, https://doi.org/10.1038/s41929-018-0085-6.
[58] C. Minke, M. Suermann, B. Bensmann, R. Hanke-Rauschenbach, Is iridium demand a potential bottleneck in the realization of large-scale PEM water electrolysis? Int. J. Hydrog. Energy 46 (2021) 23581–23590, https://doi.org/10.1016/j.ijhydene.2021.04.174.
[59] C. Spöri, C. Brand, M. Kroschel, P. Strasser, Accelerated degradation protocols for iridium-based oxygen evolving catalysts in water splitting devices, J. Electrochem. Soc. 168 (2021), 034508, https://doi.org/10.1149/1945-7111/abeb61.
[60] R. Iwata, L. Zhang, K.L. Wilke, S. Gong, M. He, B.M. Gallant, E.N. Wang, Bubble growth and departure modes on wettable/non-wettable porous foams in alkaline water splitting, Joule 5 (2021) 887–900, https://doi.org/10.1016/j.joule.2021.02.015.
[61] A.R. Zeradjanin, A.A. Topalov, Q. Van Overmeere, S. Cherevko, X. Chen, E. Ventosa, W. Schuhmann, K.J.J. Mayrhofer, Rational design of the electrode morphology for oxygen evolution-enhancing the performance for catalytic water oxidation, RSC Adv. 4 (2014) 9579–9587, https://doi.org/10.1039/c3ra45998e.
[62] T. Kwon, H. Hwang, Y.J. Sa, J. Park, H. Baik, S.H. Joo, K. Lee, Cobalt assisted synthesis of IrCu hollow octahedral nanocages as highly active electrocatalysts toward oxygen evolution reaction, Adv. Funct. Mater. 27 (2017) 1–8, https://doi.org/10.1002/adfm.201604688.
[63] J. Park, Y.J. Sa, H. Baik, T. Kwon, S.H. Joo, K. Lee, Iridium-based multimetallic nanoframe@nanoframe structure: an efficient and robust electrocatalyst toward oxygen evolution reaction, ACS Nano 11 (2017) 5500–5509, https://doi.org/10.1021/acsnano.7b00233.
[64] L. Fu, G. Cheng, W. Luo, Colloidal synthesis of monodisperse trimetallic IrNiFe nanoparticles as highly active bifunctional electrocatalysts for acidic overall water splitting, J. Mater. Chem. A 5 (2017) 24836–24841, https://doi.org/10.1039/c7ta08982a.
[65] J. Feng, L. Fang, W. Zhang, P. Li, K. Wang, C. Yang, B. Wag, Y. Yang, J. Zhou, Iridium-based multimetallic porous hollow nanocrystals for efficient overall-water-splitting catalysis, Adv. Mater. 29 (2017), 1703798, https://doi.org/10.1002/adma.201703798.
[66] V. Gridin, J. Du, S. Haller, P. Theis, K. Hofmann, G.K.H. Wiberg, U.I. Kramm, M. Arenz, GDE vs RDE: impact of operation conditions on intrinsic catalytic parameters of FeNC catalyst for the oxygen reduction reaction, Electrochim. Acta 444 (2023), 142012, https://doi.org/10.1016/j.electacta.2023.142012.
[67] M. Inaba, A.W. Jensen, G.W. Sievers, M. Escudero-Escribano, A. Zana, M. Arenz, Benchmarking high surface area electrocatalysts in a gas diffusion electrode: measurement of oxygen reduction activities under realistic conditions, Energy Environ. Sci. 11 (2018) 988–994, https://doi.org/10.1039/c8ee00019k.
[68] P. Collantes Jiménez, G. Sievers, A. Quade, V. Brüser, R.K. Pittkowski, M. Arenz, Gas diffusion electrode activity measurements of iridium-based self-supported catalysts produced by alternated physical vapour deposition, J. Power Sources 569 (2023), https://doi.org/10.1016/j.jpowsour.2023.232990.
[69] J. Schröder, V.A. Mints, A. Bornet, E. Berner, M. Fathi Tovini, J. Quinson, G.K. H. Wiberg, F. Bizzotto, H.A. El-Sayed, M. Arenz, The gas diffusion electrode setup as straightforward testing device for proton exchange membrane water electrolyzer catalysts, JACS Au 1 (2021) 247–251, https://doi.org/10.1021/jacsau.1c00015.
[70] A. Bornet, R. Pittkowski, T.M. Nielsen, E. Berner, A. Maletzko, J. Schröder, J. Quinson, J. Melke, K.M.Ø. Jensen, M. Arenz, Influence of Temperature on the performance of carbon- and ATO-supported oxygen evolution reaction catalysts in a gas diffusion electrode setup, ACS Catal. 13 (2023) 7568–7577, https://doi.org/10.1021/acscatal.3c01193.
[71] S. Trasatti, Electrocatalysis: understanding the success of DSA®, Electrochim. Acta. 45 (2000) 2377–2385, https://doi.org/10.1016/S0013-4686(00)00338-8.
[72] A. Touni, A. Papaderakis, D. Karfaridis, G. Vourlias, S. Sotiropoulos, Oxygen evolution reaction at IrO_2/Ir(Ni) film electrodes prepared by galvanic replacement and anodization: effect of precursor Ni film thickness, Molecules 24 (2019) 1–16, https://doi.org/10.3390/molecules24112095.
[73] M. Malinovic, M. Ledendecker, Whittling iridium down to size, Nat. Energy 7 (2022) 7–8, https://doi.org/10.1038/s41560-021-00963-x.
[74] A. Touni, O.A. Grammenos, A. Banti, D. Karfaridis, C. Prochaska, D. Lambropoulou, E. Pavlidou, S. Sotiropoulos, Iridium oxide-nickel-coated titanium anodes for the oxygen evolution reaction, Electrochim. Acta 390 (2021), 138866, https://doi.org/10.1016/j.electacta.2021.138866.
[75] C. Rozain, E. Mayousse, N. Guillet, P. Millet, Influence of iridium oxide loadings on the performance of PEM water electrolysis cells: Part II - Advanced oxygen electrodes, Appl. Catal. B 182 (2016) 123–131, https://doi.org/10.1016/j.apcatb.2015.09.011.
[76] C. Rozain, E. Mayousse, N. Guillet, P. Millet, Influence of iridium oxide loadings on the performance of PEM water electrolysis cells: Part I-Pure IrO_2-based anodes, Appl. Catal. B 182 (2016) 153–160, https://doi.org/10.1016/j.apcatb.2015.09.013.
[77] L.I.N. Tomé, V. Baião, W. da Silva, C.M.A. Brett, Deep eutectic solvents for the production and application of new materials, Appl. Mater. Today 10 (2018) 30–50, https://doi.org/10.1016/j.apmt.2017.11.005.
[78] D. Yu, Z. Xue, T. Mu, Deep eutectic solvents as a green toolbox for synthesis, Cell Rep. Phys. Sci. 3 (2022), 100809, https://doi.org/10.1016/j.xcrp.2022.100809.
[79] O.S. Hammond, A.V. Mudring, Ionic liquids and deep eutectics as a transformative platform for the synthesis of nanomaterials, Chem. Commun. 58 (2022) 3865–3892, https://doi.org/10.1039/d1cc06543b.
[80] E. Plaza-Mayoral, I. Jordão Pereira, K. Nicole Dalby, K. Degn Jensen, I. Chorkendorff, H. Falsig, P. Sebastián-Pascual, M. Escudero-Escribano, Pd-Au nanostructured electrocatalysts with tunable compositions for formic acid oxidation, ChemRxiv. (2022) 1–44, https://doi.org/10.1021/acsaem.2c01361.
[81] O. Kasian, S. Geiger, P. Stock, G. Polymeros, B. Breitbach, A. Savan, A. Ludwig, S. Cherevko, K.J.J. Mayrhofer, On the origin of the improved ruthenium stability in RuO_2 –IrO_2 mixed oxides, J. Electrochem. Soc. 163 (2016) F3099–F3104, https://doi.org/10.1149/2.0131611jes.
[82] M. Liu, S. Liu, Q. Mao, S. Yin, Z. Wang, Y. Xu, X. Li, L. Wang, H. Wang, Ultrafine ruthenium-iridium-tellurium nanotubes for boosting overall water splitting in acidic media, J. Mater. Chem. A 10 (2022) 2021–2026, https://doi.org/10.1039/d1ta07789a.
[83] A.L. Strickler, R.A. Flores, L.A. King, J.K. Nørskov, M. Bajdich, T.F. Jaramillo, Systematic investigation of iridium-based bimetallic thin film catalysts for the oxygen evolution reaction in acidic media, ACS Appl. Mater. Interfaces 11 (2019) 34059–34066, https://doi.org/10.1021/acsami.9b13697.